IEEE Access
Multidisciplinary ⋮ Rapid Review ⋮ Open Access Journal

Received 16 November 2023, accepted 4 December 2023, date of publication 12 December 2023,
date of current version 19 December 2023.

Digital Object Identifier 10.1109/ACCESS.2023.3341759

RESEARCH ARTICLE

Optimized Energy Management of Seaports With Integrated AMP Technology and DC Microgrid

ADIL AYUB SHEIKH, (Graduate Student Member, IEEE), AND DONG-CHOON LEE, (Senior Member, IEEE)
Electrical Engineering Department, Yeungnam University, Gyeongsan 38541, South Korea

Corresponding author: Dong-Choon Lee (dclee@yu.ac.kr)

This work was supported by the National Research Foundation of Korea (NRF) Grant funded by the Korean Government through Ministry of Science and ICT (MSIT) under Grant 2021R1A2C2005996.

ABSTRACT This paper proposes a novel multi-stage optimal economic dispatch algorithm for a seaport integrated with a DC microgrid to support the main grid while feeding local loads. In addition, a dynamic pricing profile has been generated to encourage the adoption of alternative maritime power (AMP) technology by both parties (seaports and ships). Optimum charging and discharging decisions for energy storage systems (ESSs) have been initiated based on real-time grid pricing integrated with battery energy level to develop a dynamic tariff profile. Moreover, two algorithms, a rule-based algorithm and the firefly algorithm (FA), have been used together to implement an optimized energy management system (EMS). The results demonstrated that the proposed EMS can effectively schedule ESS devices while considering the economic benefits of the system. To conduct the analysis, a seaport system connected to a 10 kV DC microgrid with two 1 MW AMPs has been considered. In addition, an optimization code has been developed using MATLAB functions, and a complete study has been performed using the MATLAB/Simulink platform. The results have shown a considerable saving in cost of about 24 - 41 % by the proposed tariff profiles.

INDEX TERMS Alternative maritime power (AMP), DC microgrid, energy management system, firefly algorithm (FA), multi-objective optimization, penalty function, rule-based optimization, seaport microgrid.

NOMENCLATURE

ABBREVIATIONS

AMP	Alternative maritime power
ESS	Energy storage system
EMS	Energy management system
RES	Renewable energy sources
BSS	Battery storage system
FC	Fuel cell
EVCS	Electric vehicle charging station
FA	Firefly algorithm
GA	Genetic algorithm
PSO	Particle swarm optimization

VARIABLES

P_{FC}	Power supplied by the fuel cell
P_b	Power supplied by the battery
P_g	Power supported by the grid
P_{PV}	Power supplied by PV system
P_{WG}	Power supplied by wind generator
P_{AMP}	Power demanded by AMP
P_{EVCS}	Power demanded by EVCS
C_{FC}	Operating cost of fuel cell
C_b	Operating cost of battery
C_g	Operating cost of grid
G_p	Real-time grid tariff rate
C_{PV}	Operating cost of PV system
C_{WG}	Operating cost of wind generator
C_{total}	Total operating cost of the system
ΔT	Optimization time interval
δ_{ch}	Binary variable representing battery charging state
δ_{dis}	Binary variable representing battery discharging state

The associate editor coordinating the review of this manuscript and approving it for publication was Hao Wang.

f_1	Represents total cost optimization function
f_2	Represents battery energy optimization function

CONSTANTS

$P_{b,c(max)}$	Maximum power rates at which battery charges
$P_{b,d(max)}$	Maximum power rates at which battery discharges
$P_{FC(max)}$	Maximum extreme power limit of fuel cell
$P_{FC(min)}$	Minimum extreme power limit of fuel cell
$P_{g(max)}$	Maximum power a grid can supply
$P_{g(min)}$	Minimum power a grid can supply
$E_{b(max)}$	Maximum energy level a battery can store
$E_{b(min)}$	Minimum energy level a battery can store
$E_{b(max\_op)}$	Maximum operating energy level for optimal operation of battery
$E_{b(min\_op)}$	Minimum operating energy level for optimal operation of battery
$P_{FC(min\_op)}$	Minimum operating power level for optimal operation of FC
P_{FC_SU}	Start up cost of FC
C_0	Penalty constant for battery system

I. INTRODUCTION

Global ship emissions have reached 1,076 million tons of CO_2 in 2018. It accounted for approximately 2.9 % of all emissions induced by human activity. Depending on long-term economic and energy assumptions, these emissions are expected to increase to 90-130 % of their 2008 levels by 2050. Consequently, the Paris Agreement aim is set to be broken if the expected growth in shipping activities that contribute to climate change persists [1], [2].

Seaport microgrids and all-electric ships (AESs) are two representative and promising technologies that have been introduced to shape the future of green maritime transportation [3]. Currently, most researchers are focusing on emission reduction when vessels are at the port, as they have a highly negative impact on residents near the port due to air pollution and noisy environment. The primary source of air emissions from ships at ports today is auxiliary diesel generators that run cargo handling machinery and other ship services (such as hoteling) while the ship stays at the port. In [4], certain important aspects of port emissions and their solutions were briefly discussed. The utilization of onshore alternative maritime power (AMP) while ships are at berth is among the best options for addressing carbon emission issues. Onshore power is also referred to as ''cold ironing'' (a term used to describe electricity provided from the shore while shutting down all the ship generators). IEEE P1713 provides a comprehensive framework for the design and operation of shore-ship connection systems, helping to ensure their safe and effective use in ports around the world [5].

Globally, several ports have already adopted AMP technology. Based on the significant changes brought on by this technology, more ports are being encouraged to adopt the same. During an average harbour stay, the port of Gothenburg can supply approximately 5 MWh of power to ferries; thus far, this has reduced SO_2 and NO emissions by 60 and 80 tons, respectively, [6]. For the installation of a shore power station, the port of Oslo has invested approximately $1.6 million. This station supplies approximately 5–6 GWh of energy annually to ferries [7]. The port of Rotterdam can satisfy a peak power demand of 1 MW, with an average power demand of 200 kW, with multiple frequencies and voltages (6.3 kV/50 Hz and 6.6 kV/60 Hz) [8]. With the combined efforts of the government and port authorities, certain main ports in South Korea began implementing AMP services in 2018. The development of this technology at these ports is progressing rapidly to achieve the goal of a 13 % reduction in fine dust by 2030. According to the International Association of Ports and Harbors (IAPH) report [9], 66 ports in 16 countries have installed cold ironing technology by 2020. The adoption of this technology is progressing rapidly, prompting a need for focused research on detailed studies related to factors such as emission footprint, economic benefits, and more.

Several studies have considered different sources of shore-side power supply to ships rather than simply the grid supply. These include mobile-cold ironing [10], liquefied natural gas (LNG)-based shore power generators [11], renewable energy sources (RES) [12], and energy storage systems (ESSs) (e.g., fuel cells and batteries). Furthermore, air pollution caused by national energy grids is among the main obstacles to employing cold ironing through the grid supply. Certain studies have concentrated on the addition of renewable generation as part of a cold-ironing project to guarantee that projects are as eco-friendly as feasible. In [13], a hybrid system that combines a 5 MW photovoltaic system with four 1.5 MW wind turbines was considered, and any surplus energy could be fed into the grid. In [12], the authors suggested a smart port microgrid that can completely use cold ironing based on RES. The proposed system at the Barcelona port can provide energy to berthed ships from wind and solar energy at approximately 75 % and 25 %, respectively. At the port of Civitavecchia [14], a 2 MWp PV system was installed to supply power to lighting, offices, and other loads. Similarly, the port of Vigo erected 100 kW of solar and wind systems under the green project initiative [11] to supply its own local load. Further, the possibility of providing power to ships at anchor using offshore wind turbines has been examined by [15]. While numerous studies have explored various sources for implementing AMP technology at seaports, a significant gap exists in justifying the benefits of AMP technology based on economic factors. Most of these studies concentrate on exploring different sources rather than emphasizing the economic rationale for implementing AMP technology.

For managing AMP-based systems, most studies have focused on voyage scheduling and berth allocation to facilitate cost benefits [16], [17], [18], or the energy management

TABLE 1. A brief classification of popular optimization techniques.

Optimization techniques			Features and limitations	References
Mathematical optimization technique		• Linear programming (LP) • Dynamic programming (DP) • Mixed integer linear programming (MILP) • Mixed integer non-linear programming (MNLP) • Mixed integer quadratic programming (MIQP) • Sequential quadratic programming (SQP)	• Deterministic and structured. • Focuses on exact solution. • Struggle with complex problems. • Suited for well defined problems. • Variable efficiency and convergence time. • Used in engineering, operation research, economics and more.	[26], [39], [40], [41], [42], [47]
Meta-heuristic optimization technique	Evolutionary based	• Genetic algorithm (GA) • Non-Dominated Sorting Genetic Algorithm II (NSGA - II) • Differential evolution (DE)	• Stochastic and versatile. • Applicable to diverse problems. • Efficient in solving complex problems. • Faster convergence time for practical solutions. • Prioritizes fast near optimal solutions. • Used in scheduling, machine learning, routing and more.	[27], [28], [43], [44], [45], [46], [47]
	Swarm intelligence based	• Particle swarm optimization (PSO) • Grey wolf optimization (GWO) • Ant colony optimization (ACO) • Firefly optimization (FA) • Artificial bee colony optimization (ABC) • BAT optimization (BOA)		

of shipboard microgrids [19], [20], [21] and land-based microgrids [22]. In contrast, studies on seaport-based microgrids are very rare. Smart seaports and land-based microgrids are almost similar, except for a few differences, such as the fact that the topology of the system changes frequently due to the ongoing docking and undocking of ships. Moreover, logistical subsystems with electrical subsystems need to be considered when using seaport microgrids [3]. In summary, smart ports contain diverse power networks with various interconnected loads and sources. In addition, both loads and renewable energy sources are intermittent. Consequently, the power flow among all units should be managed efficiently. An appropriate energy management system (EMS) can enhance the efficiency of the system and facilitate economic benefits by managing generation, demand, and ESSs under an optimized routine. A global design for managing different types of loads at ports by intelligently utilizing different combinations of ESS energies has been proposed in [23]. The results have indicated a reduction in cost and an improvement in peak shaving. The authors in [24] proposed the optimal scheduling of an ESS in microgrids via the application of a multi-objective framework. To maximize the revenue of cold ironing services, price framework-based scheduling has been mentioned in [18]. Further, energy demand has been introduced in [25] using various ship load profiles. In addition to that, the energy produced by RESs has been validated by examining the solar and wind profiles at the Cartagena port (Spain). Here, the integration of different types of RESs and Energy Storage Systems (ESSs) to establish a smart seaport structure has explored. However, the investigation into diverse power profiles based on different seasons is still required to gain a comprehensive understanding of the economic benefits of AMP technology. Moreover, to comprehend the lifespan of energy storage systems, there is a need to scrutinize the impact of operating these devices under extreme conditions further.

On the other hand, several optimization approaches or tools have been used by numerous researchers to improve EMSs and obtain their optimal schedules. A brief classification of some of the best optimization techniques for energy management is summarized in Table 1. In [26], a multi-objective framework is considered for the operational constraints of a seaport. The optimization problem has been formulated using the quadratic constrained programming model (QCP) and solved using GAMS optimization. A bat optimization algorithm (BOA) has been utilized in [27] to solve the optimization issue between wind power generation and battery storage systems. A novel genetic algorithm (GA)-driven power management strategy for a 6-bus droop-controlled DC microgrid has been developed in [28], and the results demonstrated cost savings via optimal scheduling of the units.

Apart from the above techniques, there are some other approaches adapted by researchers. In [29], a fuzzy-based multi-agent system (MAS) has been employed to manage various seaport loads, including the fluctuating power from renewable sources. The authors in [30] have chosen another approach to deal with the optimal power management of the seaport network. They have applied a communication-less multi-agent framework to achieve optimal power in the system but haven't included a cost-minimization function. A model-predictive-based approach is considered in [31] for

managing the energy of ports. In that article, uncertainties in RES have been taken into consideration and managed using battery and hydrogen energy storage systems. An algorithm based on distributed-consensus-(ADMM) is proposed in [32] for maintaining the power balance in the large seaport network. The method works by sharing the information with the nearest agents and approaching the optimal value. Despite the availability of various optimization techniques, the Firefly Algorithm (FA) offers advantages due to its exponential terms in mathematical representation, facilitating faster convergence. Additionally, tuning the exploration and exploitation parameters of the FA is considered relatively straightforward.

This study aims to provide a simple and effective EMS that supports the grid and aids in emission reduction by avoiding the operation of ships in berthing mode. Moreover, this study also encourages both ship owners and seaport owners to participate in the global initiative to reduce pollution by providing attractive tariff profiles. In the considered system, different types of RES source and load profiles are considered to analyze the robustness of EMS throughout the year. The additional novel contributions of the proposed EMS are summarized as follows:

1) The grid tariff profile is integrated with the battery energy level to improve the utilization of storage devices.

2) Fast convergence with high accuracy is achieved using the optimized results.

3) Prioritization of loads and sources is also considered while operating in island mode by feeding only critical loads.

4) Penalty functions are added to lower costs and extend the lifespan of storage devices.

The paper is organized as follows: Section II discusses the components considered in the system, and a multi-objective framework is presented in Section III. Further, the multi-stage EMS algorithm is discussed in Section IV. The results for the different scenarios are presented and discussed in Section V. Finally, conclusive remarks are discussed in Section VI.

II. DESCRIPTION OF SEAPORT DC MICROGRID

A grid-connected DC Microgrid (DCMG) is considered in this study. The sources and storage components of the system include wind generation (WG), PV arrays (PV), fuel cells (FC), and battery storage systems (BSS). As shown in Fig.1, there are several types of seaport loads: crane loads, electric vehicle charging stations (EVCS), AMPs, and other loads (lighting and miscellaneous). In addition, a hierarchical control system is considered wherein centralized communication is used to fetch local-level data for upper-level control. Table 2 lists all values of the relevant components.

A. RENEWABLE ENERGY SOURCES

The most common RESs in the microgrids are WG and PV. Apart from the installation costs, the operating costs of these sources is almost zero. In this study, therefore, maintenance costs are neglected. The PV and wind power profiles for every 10 min interval are shown in Fig. 2 and 3, respectively, for a whole year [33].

TABLE 2. System parameters.

Components	Rated Values
System Voltages	DC side : 10 kV, AC side : 6.6 kV
Wind Generation	P_{WG} : 2 MW
PV Array	P_{PV} : 1 MW
Fuel Cell (FC)	P_{FC} : 2 MW, $P_{FC(min}$: 0, $P_{FC(max)}$: 2 MW a : 0.000515 \$/kW^2, b : 0.0207 \$/kW, c : 0.2 \$
Battery (BSS)	P_b : 2 x 1 MWh, η_c : 0.9, η_d : 0.95 $P_{b,d(max)}$: 250 kW, $P_{b,c(max)}$: 200 kW $E_{b(max\_op)}$: 850 kWh, $E_{b(min\_op)}$: 200 kWh $E_{b(max)}$: 1 MWh, $E_{b(min)}$: 0 E_{b1} : 400 kWh, E_{b2} : 600 kWh
Main grid	$P_{g(max)}$: 5 MW, $P_{g(min)}$: - 2 MW
Tariff rate	Off - peak : 0.04 to 0.06 \$/kWh Mid - peak : 0.07 to 0.10 \$/kWh On - peak : 0.11 to 0.13 \$/kWh G_{p1} : 0.07 \$/kWh, G_{p2} : 0.10 \$/kWh
Loads	AMP loads - $P_{(max)}$: 2 x 1 MW Voltage : 11 kV & 6.6 kV Frequency : 50 Hz & 60 Hz
	EVCS Load - $P_{(max)}$: 1 MW
	Crane & other loads - $P_{(max)}$: 5 MW

B. FUEL CELL

Proton exchange membrane (PEM) fuel cells are considered in this study as they have a higher efficiency and a faster startup time for stationary power applications. In addition, the optimization time interval ΔT is selected to be 10 min. The fuel consumption cost of FC generators is modelled by a nonlinear relationship with the FC power. Therefore, the FC cost function [28] can be expressed as follows:

$$C_{FC} = (a.P_{FC}^2 + b.P_{FC} + c)\Delta T \tag{1}$$

where a, b, and c are the constant coefficients listed in Table 2, and P_{FC} is the power supplied by the fuel cell.

C. BATTERY STORAGE SYSTEM

A BSS can provide ancillary services and energy arbitrage in the form of synchronized reserves; however, if not operated properly, its lifetime will be reduced. A lithium-ion-based BSS is chosen for this study because it is more effective and has a higher power density than other alternatives.

To introduce an economical trade-off between the rest of the system and the BSS, (2) is introduced. As BSS is neither a source nor a load, it is a storage device; therefore, it becomes difficult to consider its operating cost for the optimization algorithm. In the actual case, BSS will only have

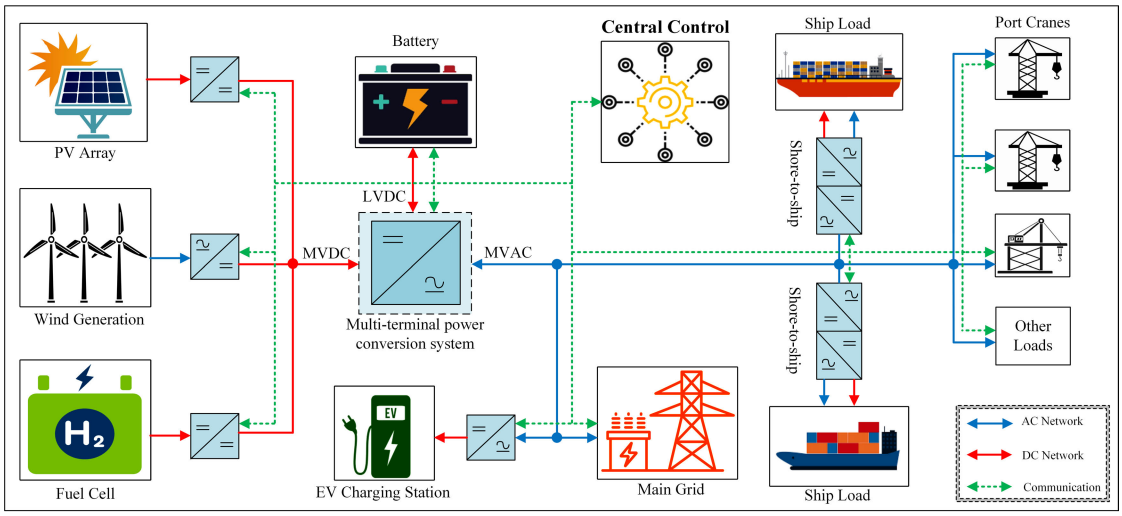

FIGURE 1. Architecture of a seaport integrated with DC microgrid.

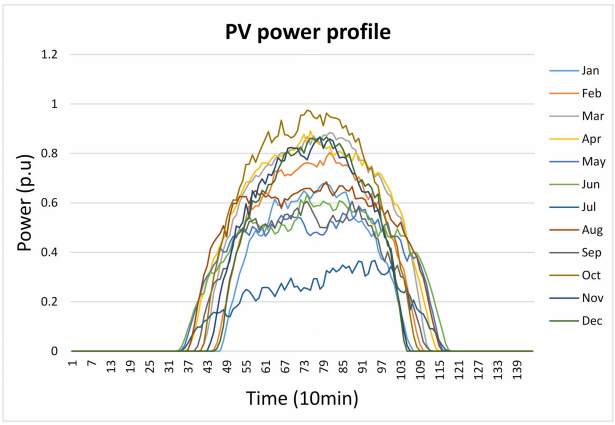

FIGURE 2. PV power profile for a whole year (10 min × 24h).

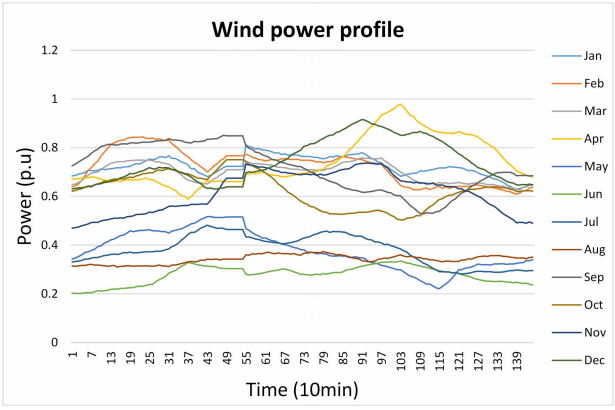

FIGURE 3. Wind power profile for a whole year (10 min × 24h).

an installation cost, and the operating cost will be almost zero throughout its lifetime. So, to include the BSS cost function in the optimization algorithm, a cost function is utilized in such a way that it aids in maximizing the battery lifetime by managing charging and discharging cycles. A detailed derivation for the cost function has been presented in [34]. To elaborate further, charging costs will be positive and discharging costs will be negative, so in one complete cycle, the operating cost will be zero. However, during charging and discharging times, the cost values will help in finding the best optimized value. The cost function of BSS is expressed as [34]

$$C_b = \frac{694 * C_{b,CC}}{\eta_b^2 E_{b,rated} DoD(t)^{0.795}} P_b(t) \Delta T \tag{2}$$

$$DoD(t) = 1 - SoC(t) \tag{3}$$

where $C_{b,CC}$ is the capital cost of the BSS, $E_{b,rated}$ is the rated capacity of the BSS, and η_b is efficiency of the BSS. The SoC and DoD represent the state of charge and depth of discharge of the BSS, respectively. The energy stored in the BSS at instant t is expressed as

$$E_b(t) = E_b(t_0) - \left[\eta_c P_b(t_0)(-\delta_{ch}) + \frac{P_b(t_0)(\delta_{dis})}{\eta_d}\right]\Delta T \tag{4}$$

where t and t_0 are the values at the present and past time steps, respectively, η_c and η_d are the efficiencies of the battery during the charging and discharging cycles, respectively, and P_b and E_b are the power and energy of the BSS, respectively. The significance of δ_{ch} and δ_{dis} are discussed in Section IV.

D. UTILITY GRID

Smart-grid technologies have provided consumers with access to real-time electricity prices through communication. The operating cost of the main grid depends on real-time tariffs. Therefore, the operating cost of the grid (C_g) is expressed as

$$C_g = G_p P_g \Delta T \tag{5}$$

where G_p is the real-time electricity price and P_g is the power supported by the grid.

E. LOADS

As discussed earlier, in this system, four different types of loads are considered: alternate maritime power (AMP), cranes, EVCS, and other miscellaneous loads. As mentioned in [23], at the Port of Long Beach, different types of cranes are considered, such as rubber-tyred gantry (RTG), shore-to-ship (STS), and rail-mounted gantry (RMG), and at that port, about 70 % of total power demand is consumed by crane loads (31.5 % RTG, 36.6 % for STS, and 2.7 % RMG), and approx. 18 % is consumed by 'reefers' (refrigerated container in which goods are transferred). Whereas, AMP requires around 10 % of total power, and other miscellaneous loads are around 2 %.

In our considered system, these data have been adapted. To simplify the analysis, different crane load profiles and miscellaneous loads are grouped into a single crane load profile, as shown in Fig. 7(a), 7(b), 8(a), and 8(b). The rated values of different loads are listed in Table 2.

III. MULTI-OBJECTIVE PROBLEM FORMULATION

A. OBJECTIVE FUNCTION

This study involves two main objectives. The first is to minimize the overall operating cost of the system by intelligently operating the BSS and FC systems based on the main grid tariff profile. Thus, the DC microgrid can support the main grid by reducing its net operating costs. The total cost optimization function is expressed as:

$$f_1 = min\{C_{total}\} = min\{C_g + C_{FC} + C_b + C_{PV} + C_{WG}\}. \tag{6}$$

The second objective function is to maximize the stored energy in the BSS. This function will preferably attempt to maintain the SoC of the BSS at a higher energy level, and it is expressed as

$$f_2 = max\{E_b\}. \tag{7}$$

B. PROBLEM CONSTRAINTS

1) POWER BALANCE

Two main types of constraints are considered. The first constraint is related to the power balance of the overall system and is expressed as:

$$\begin{aligned} &P_g + P_{FC} + P_b(-\delta_{ch}) + P_b(\delta_{dis}) + P_{PV} + P_{WG} \\ &\quad = P_{AMP} + P_{EVCS} + P_{other\_loads}. \end{aligned} \tag{8}$$

where P_{other_loads} represents total crane loads and other miscellaneous loads.

2) OTHER CONSTRAINTS

The other constraint is the limit for all dispatchable units. Establishing these limits is crucial for optimization, preventing irrelevant and impractical results. The power supplied by each dispatchable unit should be maintained within the specified limits, which can be expressed as

$$P_{b,c(max)}(-\delta_{ch}) \le P_b \le P_{b,d(max)}(\delta_{dis}) \tag{9}$$

$$P_{FC(min)} \le P_{FC} \le P_{FC(max)} \tag{10}$$

$$-P_{g(max)} \le P_g \le P_{g(max)} \tag{11}$$

$$E_{b(min)} \le E_b \le E_{b(max)} \tag{12}$$

where $P_{b,c(max)}$, $P_{b,d(max)}$, and $P_{FC(max)}$ are the maximum power rates at which the respective components can supply or consume power at time ΔT. Further, $P_{g(max)}$ and $P_{g(min)}$ are the maximum and minimum limits of grid power, respectively, and $E_{b(max)}$ and $E_{b(min)}$ are the extreme limits that a BSS can practically have.

C. PENALTY FUNCTIONS

In this work, penalty functions are used only to avoid the extreme operating values of the optimization algorithms for FC and BSS during normal operation. The penalty functions are not designed to deal with contingency scenarios.

1) FUEL CELL

A penalty function for FC is introduced to avoid frequent shutdowns and startups. It is expressed as

$$P^n_{FC} = \begin{cases} P_{FC\_SU} & \text{if } P_{FC} \le P_{FC(min\_op)} \\ 0 & otherwise \end{cases} \tag{13}$$

where P_{FC_SU} is the startup cost, which can be in the range of \$ 2 - 5, and the minimum operating $P_{FC(min\_op)}$ value is set as 50 kW.

2) BATTERY

In Section III-B2, extreme limits for the operation of BSS are presented; however, extreme discharge and charge should be avoided usually and preferred only in the worst-case scenarios. Because charging the BSS at 100 % level and discharging it fully to 0 % makes the life span of the BSS shorter. Therefore, to avoid this in normal operating cases, the minimum and maximum operating limits $E_{b(min\_op)}$ and $E_{b(max\_op)}$, respectively, are introduced as follows:

$$P^n_b = \begin{cases} C_0 & \text{if } E_{b\_(min)} \le E_b \le E_{b(min\_op)} \\ 0 & \text{if } E_{b(min\_op)} \le E_b \le E_{b(max\_op)} \\ C_0 & \text{if } E_{b(max\_op)} \le E_b \le E_{b(max)} \end{cases} \tag{14}$$

where C_0 is a constant selected to avoid overcharging and extreme discharging in normal scenarios. Based on the understanding of the system, it can be selected between \$10 to 12. All the respective values are listed in Table 2.

IV. PROPOSED MULTI-STAGE EMS ALGORITHM

The proposed EMS algorithm assumes a hierarchical control architecture wherein EMS decisions are explained in three stages, as follows:

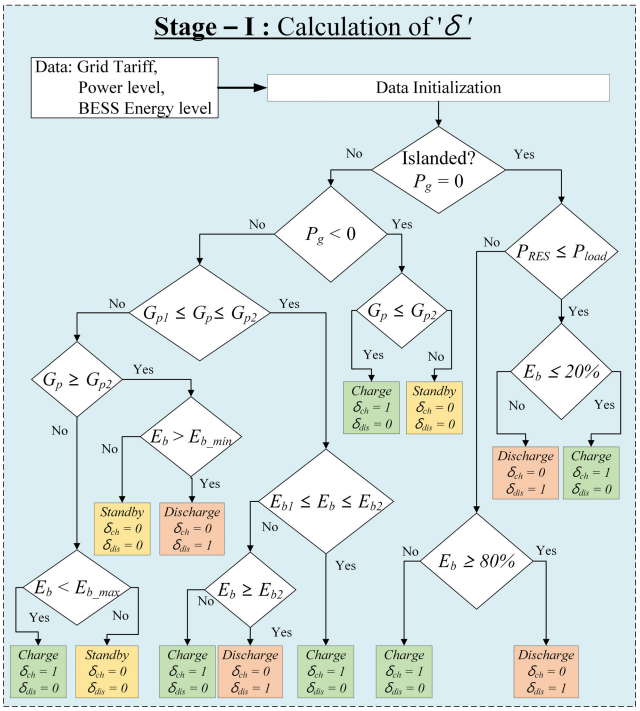

FIGURE 4. Flowchart for Stage I: Calculation of variable δ.

A. STAGE I

In Stage I, a rule-based algorithm is used. The set of rules is designed such that it optimizes the energy stored in the battery based on the grid tariff when the system is in grid-connected mode and based on the threshold when it is operated in islanded mode, as shown in Fig. 4. Here, P_g, G_p, and E_b represent grid power, grid energy price, and energy stored in the BSS, respectively. All the respective boundary values are listed in Table 2 and selected based on understanding of the system. Moreover, δ_{ch} and δ_{dis} are binary variables that denote the state in which the battery operates, such as charging ($\delta_{ch} = 1$ and $\delta_{dis} = 0$), discharging ($\delta_{ch} = 0$ and $\delta_{dis} = 1$), or on standby ($\delta_{ch} = 0$ and $\delta_{dis} = 0$). There are in total three standby modes. The standby mode (when $P_g < 0$) is included to avoid battery discharge while feeding extra power to the grid, as supplying the grid from the battery is not recommended for the considered system. Moreover, two other standby modes are added to avoid overcharging and deep discharging of the battery. When the system is operated in islanded mode, the battery charging decision is made based on a pre-determined threshold. Consequently, this Stage I decision, along with other parameters, is passed on to Stage II.

B. STAGE II

In Stage II, the FA optimization algorithm is used as it offers several advantages over the other popular optimization techniques, like GA and particle swarm optimization (PSO). For the considered system, the EMS algorithm is tested using the FA, GA, and PSO. In most cases, the results are the same, as can be observed in Table 4. However, the computation burden (convergence time) is higher in the GA and PSO compared with the FA, as shown in Fig. 12, which is why the FA optimization technique is chosen for this study. The reason behind the faster convergence of FA is its inherent property of dividing fireflies into subgroups based on their respective locations. In addition, the randomness variable can also be tuned with the iterations, which helps accelerate the optimization and achieve faster convergence [35].

1) FIREFLY ALGORITHM

In this subsection, a brief introduction to the FA is described, and a detailed theory can be found in [35]. This algorithm is a meta-heuristic algorithm inspired by nature and randomness and is used in almost all swarm group intelligence methods. In FA, light intensity (brightness) and attraction are two important variables. Fireflies that are less bright are absorbed by the firefly that is brighter than them, where the brightness is determined by objective functions. Moreover, attraction is dependent on brightness, which increases as fireflies move towards each other and vice versa. The objective function accepts a list of D parameters (variables to be optimized) as inputs and returns a scalar value representing the fitness of the solution. For the movement of the fireflies, the new position of each firefly is updated as

$$X_i^t = X_i^{t_0} + \beta e^{-\gamma r_{ij}^2}(X_j^{t_0} - X_i^{t_0}) + \alpha^{t_0}\varepsilon_i^{t_0} \quad (15)$$

$$r_{ij} = X_j^{t_0} - X_i^{t_0} \quad (16)$$

$$\alpha^{t_0} = \alpha_0 \delta^{t_0}, \quad 0 < \delta < 1 \quad (17)$$

where α, β, and γ are the randomness strength, attractiveness, and absorption factors, respectively. These three factors are the tuning parameters that control the exploration and exploitation behaviors of the algorithm. Here, δ is the randomness reduction factor, and ε is the distribution function. In this study, these variables of FA are finely tuned based on the trial-and-error method to avoid premature convergence. Further, $X_i^{t_0}$ and $X_i^{t_0}$ are the positions of the 'i_{th}' and 'j_{th}' fireflies at t_0 instant, respectively. The equation contains an exponential term, which facilitates faster convergence of the FA compared to standard optimization algorithms.

2) OPTIMIZATION

Based on the Stage I decision and initial values, the FA attempts to determine the optimal scheduling parameters until it reaches the optimum values, as shown in Fig. 5. In the algorithm, fireflies move towards each other based on intensity using (15), and a new solution is calculated. Subsequently, the upper bounds (UB) and lower bounds (LB) expressed (9)-(12) are checked to limit the fireflies within the defined boundary of the optimization variables. Thereafter, the light intensity of the local best firefly is updated, and this process is repeated until the maximum number of iterations (i_max) is reached. The algorithm gets terminated if no higher-intensity fireflies exist in the search space. Once the optimization converges, the solutions are stored in the memory. Further, the best possible objective

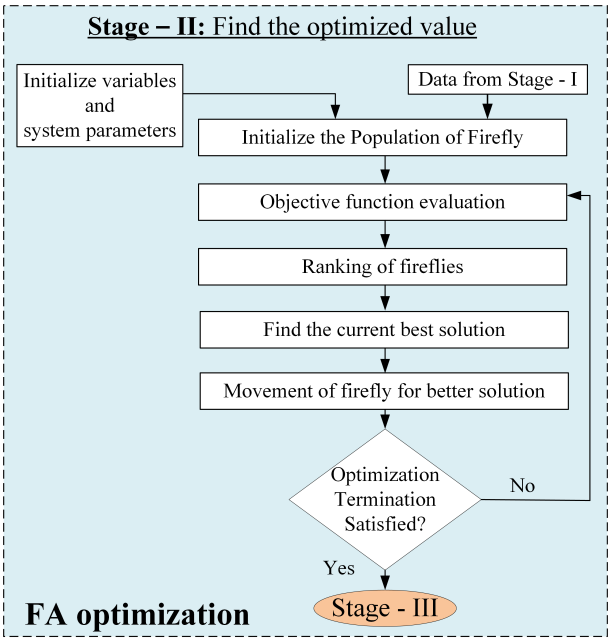

FIGURE 5. Flowchart for stage II: Finding the optimized values.

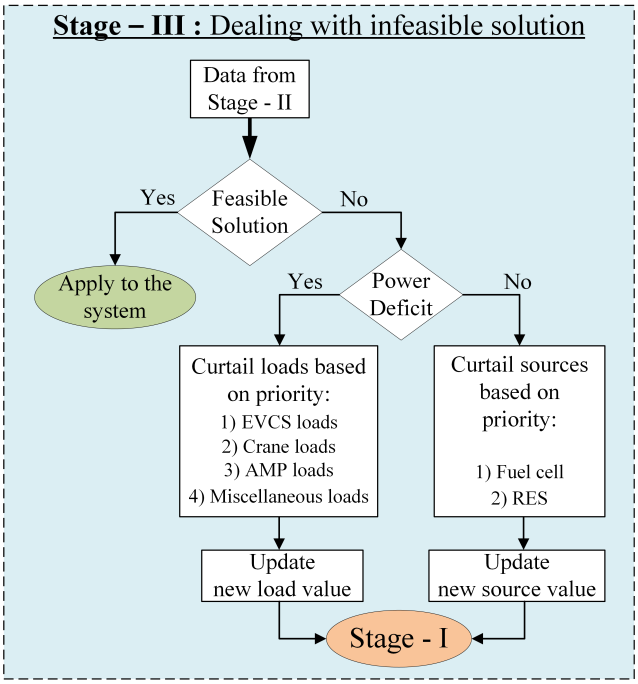

FIGURE 6. Flowchart for stage III: Dealing with infeasibility.

values of $min(C_{total})$ and $max(E_b)$, and the optimized values of P_g, P_{FC}, and P_b are shared with a lower level of control. The local level considers these values as a power reference for the dispatchable units and applies them to the respective dispatchable units. The operation of local-level control is beyond the scope of this study.

C. STAGE III

In Stage III, a rule-based approach is used (Algorithm 1) to address the infeasible solution provided by the optimization algorithm. In case of any violation of (8)-(12), the optimization algorithm cannot provide an optimized solution. Such a violation may occur due to of infeasibility caused by either a power deficit or a power surplus. Therefore, to overcome this, proper load and source curtailment based on the priority of the loads and sources is necessary, as shown in Fig. 6. The power curtailment is chosen as ≤ 100 kW for the sources and loads, based on the understanding of the system. Therefore, at every iteration of Stage III, utmost 100 kW of power will be curtailed. Following the curtailment decision, Stage I is initiated again, and the optimized values are recalculated. This entire process is repeated until a proper power balance

Algorithm 1 EMS Algorithm for Stage - II and III

Input: Stage -I parameters, UB and LB
Output: f_1, f_2, P_g, P_{FC} and P_b
Initialization: No. of fireflies (N) = 100,
D = 3, $\alpha_0 = 1.0$, $\beta = 1.0$,
$\gamma = 0.01$, $\delta = 0.97$, i_max = 100

1: **while** x=0 **do**
Generating the initial population
`// Stage-II: FA main loop`
2: **for** iteration = 1:i_max **do**
.
`// Evaluate the objective function`
3: **for** i = 1:N **do**
4: **for** j = 1:N **do**
- Move the firefly 'i' to 'j'
- Evaluate the new solution
- Check the boundary conditions
- Update the light intensity
5: **end for**
6: **end for**
Memorize the best firefly
7: **end for**
Get the global best firefly
`// Stage-III: Dealing with infeasibility`
8: **if** Infeasible results? **then**
9: x = 0; `// Require updation - repeat the while loop`
10: **if** Power deficit? **then**
11: Reduced the Load based on the priority
12: **else**
13: Reduced the sources based on the priority
14: **end if**
15: **else**
16: x = 1; `// No updation - terminate the while loop`
17: **end if**
18: **end while**
Terminate the algorithm and apply the optimized values to the system.

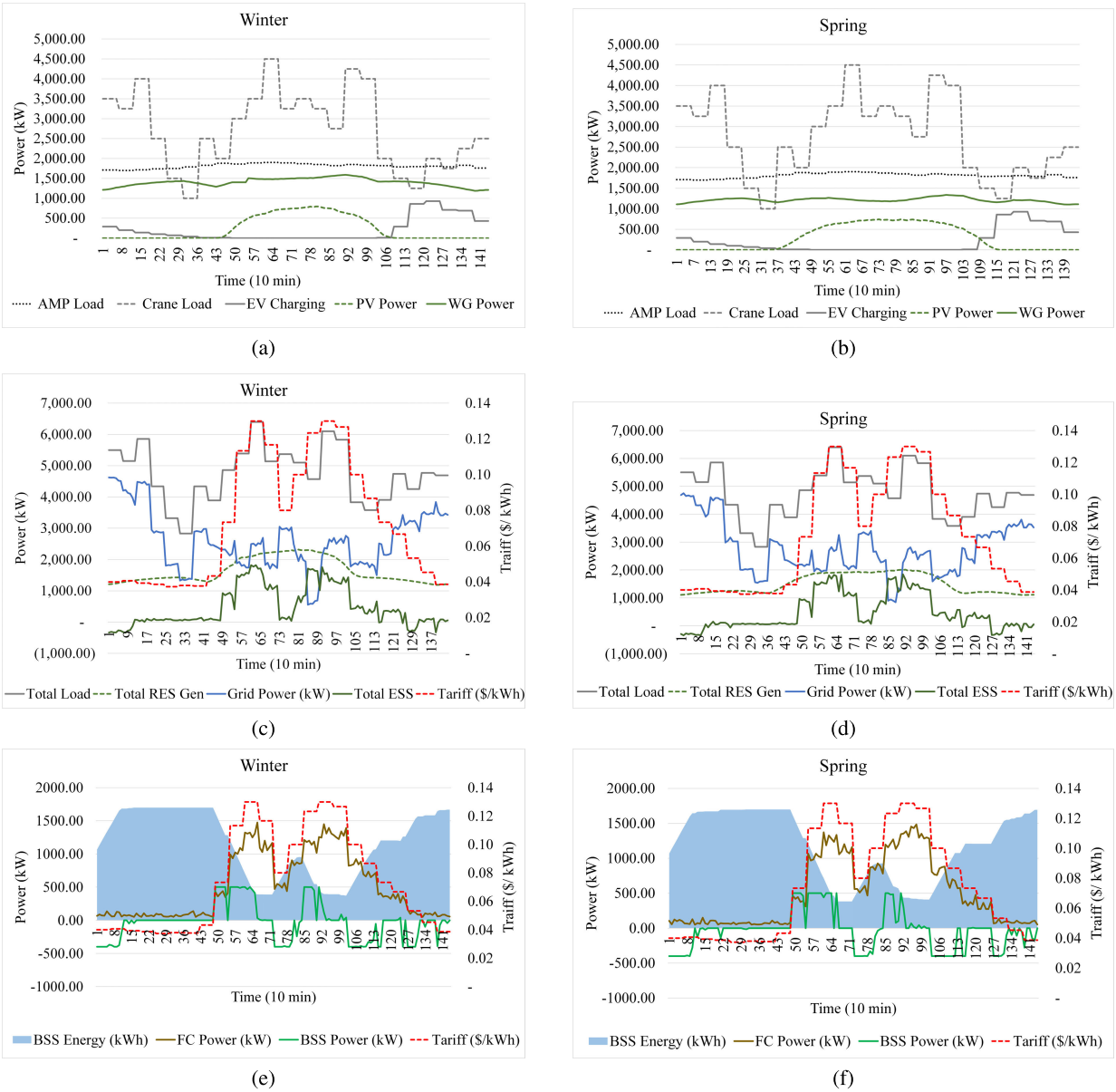

FIGURE 7. Optimization results for winter and spring seasons respectively. (a) - (b) Power profiles of PV, wind, grid, and different loads. (c) - (d) Power profiles of total load, total RES, ESSs, and tariff profile of grid. (e) - (f) Power profiles of both the ESSs and energy profiles of the BSS.

is achieved in the system and the optimization algorithm provides feasible results.

V. RESULTS AND DISCUSSIONS

A. OVERALL RESULTS FOR FOUR DIFFERENT SEASONS

In this study, four different seasonal profiles are considered to authenticate the proposed EMS for whole-year RES profiles. Every 10 min interval data of irradiance, temperature, and wind are collected for the port of Busan [33].

Furthermore, the grid tariff profile from the State Electricity Board [36] is considered for industrial loads. However, owing to the unavailability of load profiles for this port, it was adapted from [12] and [23]. Fig. 7(a), 7(b), 8(a) and 8(b) show a 24 h profile (24 h × 10 min = 128 instants) for loads and RESs for each season. Here, the average power profile is considered for each season compared to those shown in Fig. 2 and 3. The contributions by both the ESSs and the grid with respect to the tariff profile (red dotted line) are depicted in Fig. 7(c), 7(d), 8(c), and 8(d).

The power supplied by each ESS and the energy stored in the BSS are shown in the Fig. 7(e), 7(f), 8(e), and 8(f). The initial energy in each BSS is considered as 500 kWh, and throughout the day, the battery energy profile varies based on the load and grid tariff profiles. The BSS charges during off-peak hours, specifically at night, and uses this stored energy to feed loads during peak hours. During the period (9 - 18 h),

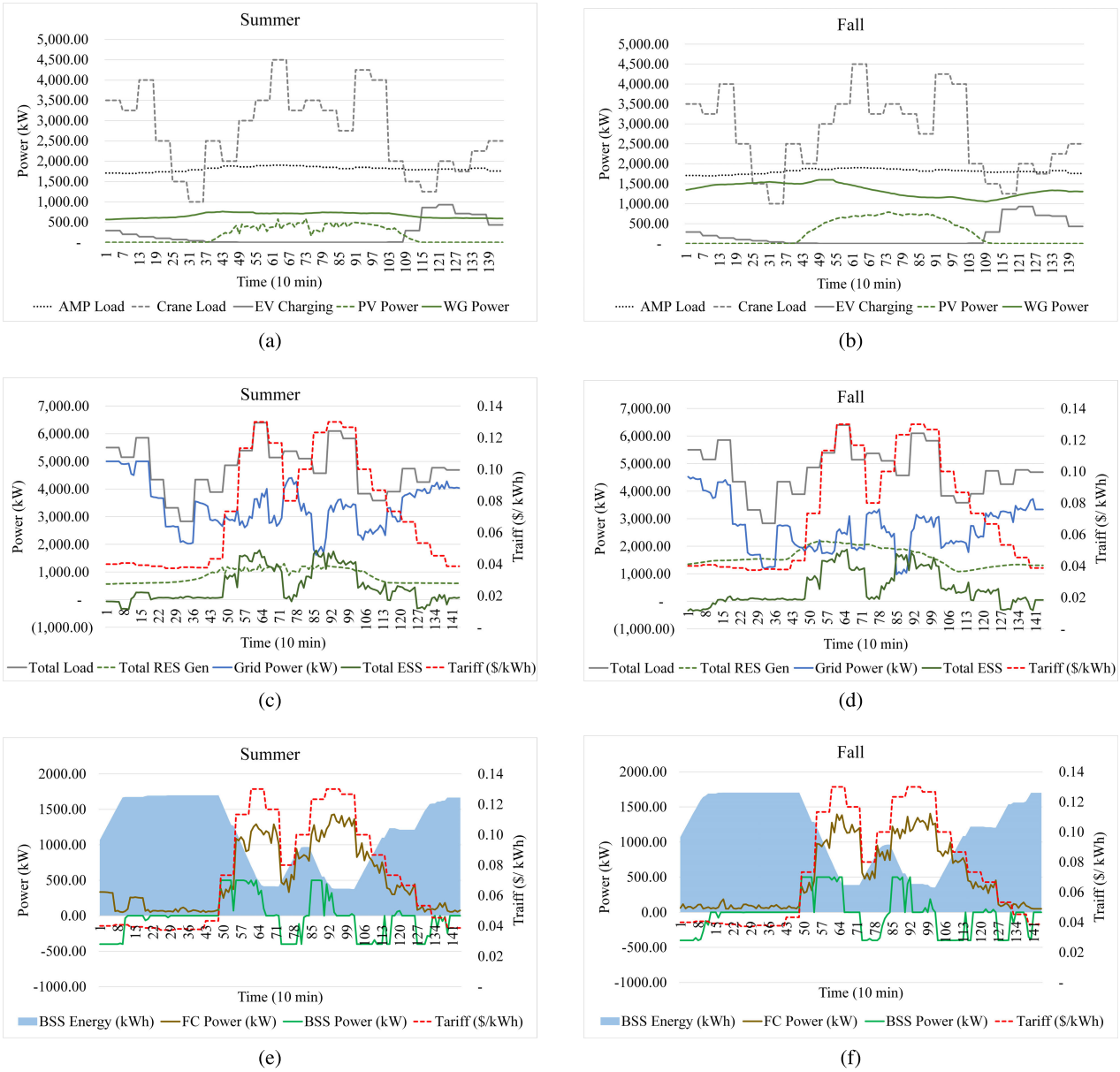

FIGURE 8. Optimization results for summer and fall seasons respectively. (a) - (b) Power profiles of PV, wind, grid, and different loads. (c) - (d) Power profiles of total load, total RES, ESSs, and tariff profile of grid. (e) - (f) Power profiles of both the ESSs and energy profiles of the BSS.

the battery energy is mostly discharged, demonstrating grid support. Subsequently, as the grid price decreases, the battery begins to charge again to regain its maximum value. However, the FC plays an important role in supporting the grid during peak hours. It contributes to the system when the grid prices are extremely high, which helps reduce the overall operating costs and provide grid support.

B. SIMULATION RESULTS FOR SELECTED CASES

To test the proposed algorithm, a model based on average modelling is developed in a MATLAB/Simulink environment, as shown in Fig. 1. The optimization code is implemented in a MATLAB function, and the respective optimized power references are generated for dispatchable components. The algorithm is tested for certain special cases, as shown in Fig. 9:

1) CASE 1: FLUCTUATION IN RES

In case 1, high penetrations from both the RES with fluctuation in power support (1.5 - 4.5 s) are considered. Here, the total load and grid tariff are considered to be constant.

2) CASE 2: LESS PENETRATION FROM RES

In this case, low penetrations from both the RES with power fluctuation (6 - 9 s) are considered. Here, the load and tariff are fixed, which results in greater contributions from the grid.

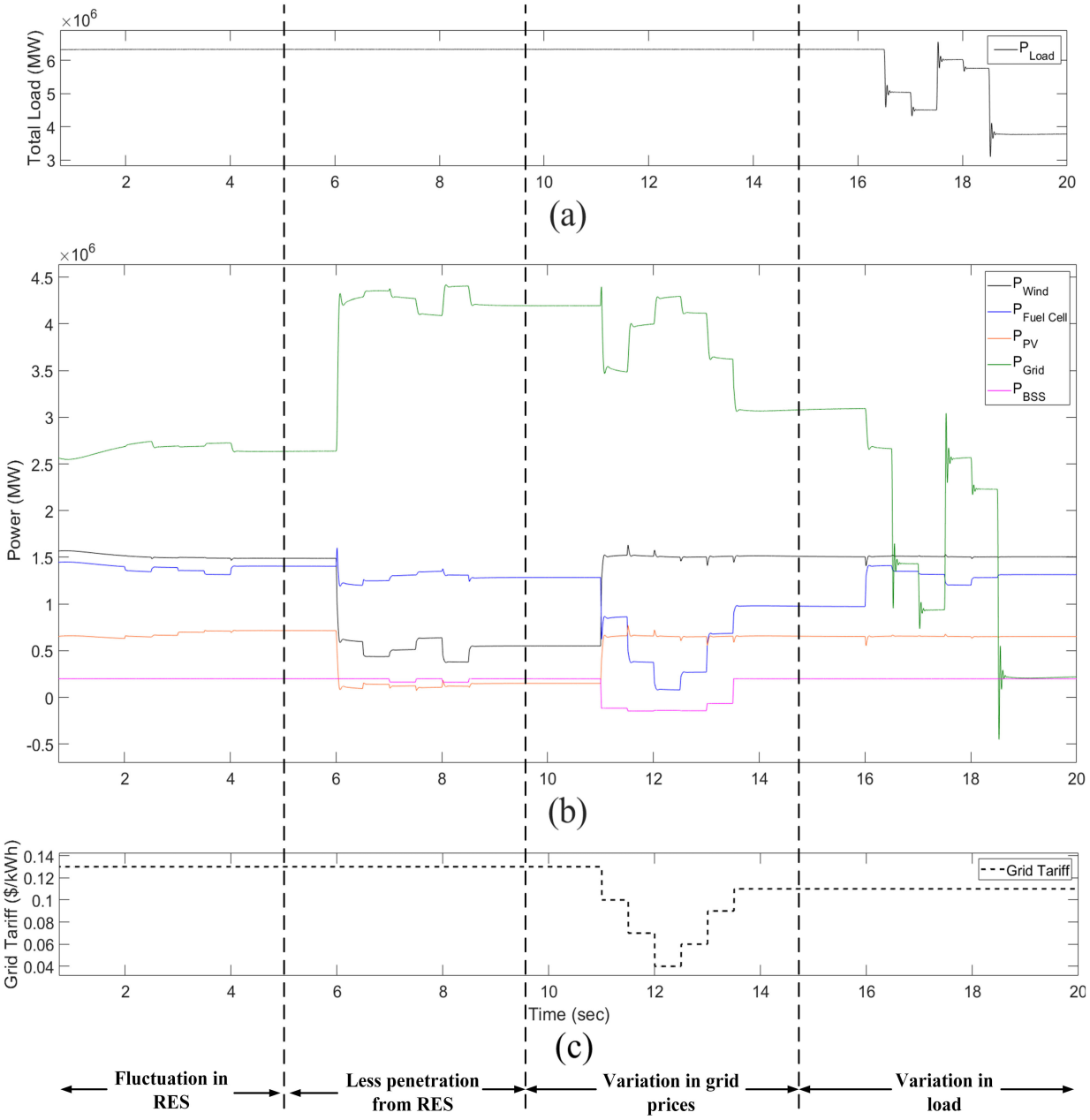

FIGURE 9. Power and tariff profiles of respective components for four different cases. (a) Variation in load power. (b) Power contribution from the respective components. (c) Variation of grid tariff.

3) CASE 3: VARIATION IN GRID PRICES

In case 3, variation in grid prices is considered by maintaining the RES contribution similar to that in case 1 (11 - 14 s). Based on the grid tariff profile, both the ESSs changed their support for the system.

4) CASE 4: VARIATION IN LOAD

Variation in load having fixed grid tariff (16 - 19 s) is considered.

The proposed system can adapt electrical parameters based on ship requirements. In the above cases, AMP-1 is considered to operate at an 11 kV/ 50 Hz supply, whereas AMP-2 operates at a 6.6 kV/ 60 Hz supply. Here, at 17.5 s, load from AMP-1 increases, whereas at 18 s, that from AMP-2 decreases, as shown in Fig. 9(a) and 10. The voltage, current, and frequency profiles are shown in Fig. 10.

C. COST ANALYSIS AND BENEFITS

Installation and operating costs are major hurdles for adapting AMP technologies worldwide. There are mainly two parties involved: the seaport authority and ship owners. To facilitate

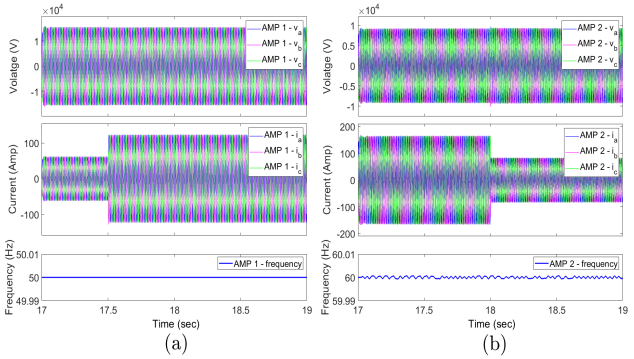

FIGURE 10. Step load change in the AMPs. (a) Increase in AMP-1. (b) Decrease in AMP-2.

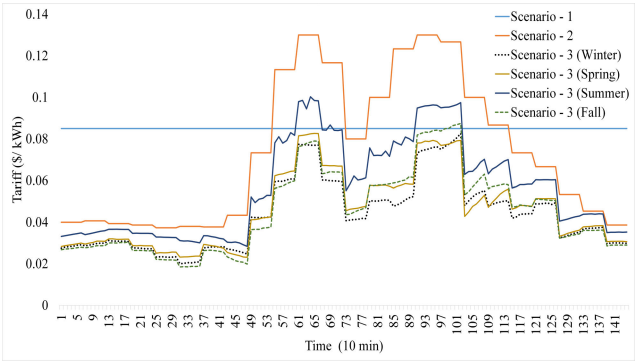

FIGURE 11. Dynamic tariff profiles for different scenarios (10 min).

an ethical trade-off between them, a better tariff price must be decided. Economic tariffs encourage their participation in the initiative to install AMP. As discussed previously, the primary focus of this study is on the operating costs of the system; all other costs are beyond the scope of this study. For a fair comparison, the following three scenarios are considered:

- Scenario 1: Selling power to the ship owner through AMP at a fixed tariff (only grid supply).
- Scenario 2: Selling power to the ship owner at real-time grid tariffs (only grid supply).
- Scenario 3: Selling power to the ship owner from the proposed system having dynamic selling price (varied based on the availability of seaport RESs, ESSs, loads, and grid prices).

Scenario 2 is only beneficial for the ship owner and motivates them to participate in this initiative. Whereas, Scenario 3 will encourage both parties to participate since it has control over several local components, which facilitates the economic management of local loads and provides a better tariff to the ship user. Moreover, the proposed optimized system can ensure a stable and reliable power supply for the ship even during the islanded mode of operation of the seaport.

The comparative tariff profiles for different seasons and scenarios are illustrated in Fig. 11. As evident, the different profiles indicate that well-optimized power support can assist in reducing grid peaks during peak hours and provide dynamic pricing to the consumer. The operating costs in Scenarios 2 and 3 for different seasonal profiles are listed in Table 3. Considerable reductions in the operating costs for Scenario 3 in winter, spring, and fall of approximately 41 %, 38 %, and 39 %, respectively, can be observed. Whereas, for summer, a reduction of approximately 23.5 % was achieved since changes in the grid tariff profile for different seasons are not considered to avoid complications. However, the results in Scenario 1 cannot be compared in Table 3, as they are strictly related to ship loads, although both ship and seaport loads are considered in this study.

TABLE 3. Operating cost for 24 h profile.

Time (hour)	Scenario 2	Scenario 3			
		Winter	Spring	Summer	Fall
1	$ 220.00	$ 156.25	$ 160.40	$ 187.19	$ 150.58
2	$ 209.43	$ 151.64	$ 156.48	$ 180.37	$ 145.96
3	$ 230.34	$ 181.07	$ 186.69	$ 214.24	$ 176.72
4	$ 167.81	$ 119.03	$ 124.54	$ 150.41	$ 114.48
5	$ 123.95	$ 77.28	$ 84.30	$ 108.72	$ 72.85
6	$ 107.54	$ 58.00	$ 66.44	$ 87.00	$ 52.86
7	$ 163.76	$ 121.66	$ 123.77	$ 142.52	$ 113.76
8	$ 168.57	$ 101.37	$ 94.05	$ 115.88	$ 83.55
9	$ 356.40	$ 205.66	$ 203.38	$ 251.10	$ 179.63
10	$ 610.87	$ 323.81	$ 342.42	$ 432.19	$ 312.69
11	$ 832.00	$ 493.64	$ 525.84	$ 627.25	$ 498.49
12	$ 599.67	$ 307.80	$ 344.86	$ 435.04	$ 328.31
13	$ 429.60	$ 222.03	$ 250.59	$ 320.27	$ 242.81
14	$ 510.00	$ 257.12	$ 293.83	$ 372.03	$ 295.47
15	$ 563.63	$ 228.74	$ 263.95	$ 360.85	$ 275.35
16	$ 793.00	$ 457.12	$ 479.82	$ 584.30	$ 507.52
17	$ 615.39	$ 380.89	$ 378.89	$ 465.85	$ 415.95
18	$ 383.00	$ 200.19	$ 183.78	$ 253.31	$ 222.10
19	$ 310.27	$ 176.60	$ 186.53	$ 240.26	$ 205.79
20	$ 286.44	$ 169.53	$ 185.46	$ 225.39	$ 186.52
21	$ 315.87	$ 232.04	$ 243.21	$ 286.03	$ 240.46
22	$ 226.77	$ 144.03	$ 147.94	$ 177.71	$ 141.96
23	$ 216.24	$ 177.34	$ 181.78	$ 209.60	$ 172.26
24	$ 181.35	$ 140.28	$ 144.27	$ 164.95	$ 135.69
Total	$ 8621.89	$ 5083.08	$ 5353.22	$ 6592.45	$ 5271.77
% Saving		41.04 %	37.91 %	23.53 %	38.85 %

It has been mentioned in the IMO resolution MEPC.32(74) [9] that voluntary cooperation is necessary between ports and ship owners to reduce the impact of greenhouse gas (GHG) emissions and that RES should preferably be used as an alternative onshore power supply. However, in the current scenario, cold ironing technology appears to be a costlier alternative for the reason that the installation cost is much higher. Despite the awareness regarding the potential of this technology, widespread adoption is hindered due to its economic boundaries. It was mentioned in [37] and [38] that this technology is currently not economically feasible compared to most EU countries. Adaptation depends on several factors, such as fuel prices, electricity prices, geographical location, and government policies. In the future,

TABLE 4. Optimization results for winter season (10 min time interval) by GA, PSO and FA optimization techniques.

	GA	PSO	FA
No. of iterations	100	100	100
Cost optimization function (f_1)	\$ 82.1	\$ 82.15	\$ 82.15
BSS energy level function (f_2)	389.3 kWh	391.1 kWh	390.38 kWh
Fuel cell Power (P_{FC})	1473.04 kW	1474.8 kW	1475.21 kW
BSS power (P_b)	36.64 kW	35.29 kW	35.38 kW
Grid power (P_g)	2694.1 kW	2693.69 kW	2693.19 kW

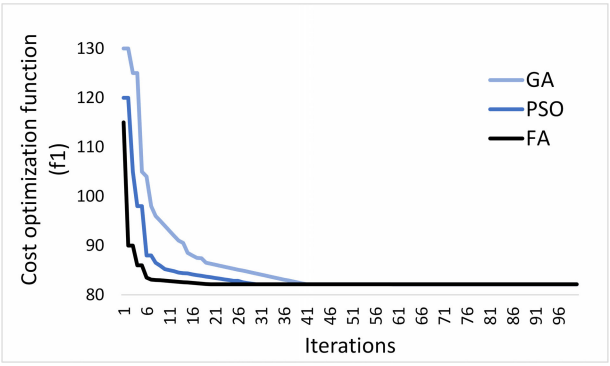

FIGURE 12. Convergence curve of GA, PSO and FA optimization techniques.

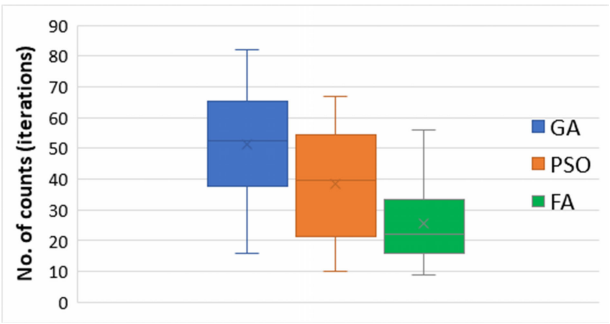

FIGURE 13. Box plot of GA, PSO and FA optimization techniques.

the situation may change if governments provide subsidies and incentives for installation.

D. COMPARISON BETWEEN GA, PSO, AND FA

In this subsection, a comparison is made among the three most popular meta-heuristic optimization techniques. For all three methods, the total number of iterations is considered to be 100. Upon examining Table 4, it can be observed that all these techniques yield almost identical optimal solutions. This proves that a global optimal solution has been achieved using firefly algorithm. However, FA exhibits faster convergence compared to the other two methods, as illustrated in Fig. 12. The GA and PSO reach the optimal solution in 41 and 28 iterations, respectively, whereas the FA reaches the global optimal solution in just 16 iterations. Moreover, to showcase the number of iterations for each optimization technique considering all the cases a box plot is depicted in Fig. 13. This demonstrates the superiority of the FA technique over the GA and PSO techniques in terms of achieving the optimal solution more quickly for the considered optimization problem.

VI. CONCLUSION

This study proposed a multi-stage EMS scheme to facilitate efficient dispatch of the seaport DC microgrid components and reduce operational costs. The results demonstrated that the heuristic method based on the FA in collaboration with a rule-based algorithm facilitated more efficient optimization of the DC microgrid components. The proposed optimization algorithm effectively optimized the dispatchable components of a DC microgrid. It has shown that the BSS consumed and supplied power more intelligently, particularly during off-peak and peak hours of the grid. In addition, a dynamic pricing profile has been generated for different seasons to economically benefit both consumers (ports and ships). Finally, benefits in operating costs are observed while fulfilling seaport demand by optimizing the DC seaport components rather than relying solely on grid-supplied power. The results of Scenario 3 compared to Scenario 2 revealed significant reductions in operating costs approximately 41 %, 38 %, 39 % and 23.5 % for winter, spring, fall, and summer seasons, respectively. As the system component rating varies widely based on geographical location, the proposed EMS is flexible enough to be scaled for any other up- or down-scaled system.

REFERENCES

[1] *Reducing Emissions From the Shipping Sector*. www.climate.ec.europa.eu. Accessed: Feb. 5, 2023. [Online]. Available: https://climate.ec.europa.eu/eu-action/transport-emissions/reducing-emissions-shipping-sector_en

[2] International Maritime Organization. (2021). *Fourth IMO GHG Study 2020*. [Online]. Available: https://wwwcdn.imo.org/localresources/en/OurWork/Environment/Documents/Fourth%20IMO%20GHG%20Study%202020%20-%20Full%20report%20and%20annexes.pdf

[3] S. Fang, Y. Wang, B. Gou, and Y. Xu, "Toward future green maritime transportation: An overview of seaport microgrids and all-electric ships," *IEEE Trans. Veh. Technol.*, vol. 69, no. 1, pp. 207–219, Jan. 2020, doi: 10.1109/TVT.2019.2950538.

[4] T. P. V. Zis, "Prospects of cold ironing as an emissions reduction option," *Transp. Res. A, Policy Pract.*, vol. 119, pp. 82–95, Jan. 2019, doi: 10.1016/j.tra.2018.11.003.

[5] Y. Khersonsky, N. Hingorani, and K. L. Peterson, "IEEE electric ship technologies initiative," *IEEE Ind. Appl. Mag.*, vol. 17, no. 1, pp. 65–73, Jan. 2011, doi: 10.1109/MIAS.2010.939429.

[6] A. Wilske and C. Agren. (2008). *Shore Connected Electricity Supply to Vessels in the Port of Gothenburg, Pronet*. [Online]. Available: http://www.eltis.org/sites/default/files/casestudies/documents/15_5.pdf

[7] P. G. Rekdal, "Onshore power supply Oslo pilot—HVSC in port of Oslo," in *Proc. CleanShip Conf.*, Trelleborg, Sweden, Sep. 2013, pp. 1–35.

[8] S. Doves, "Alternative maritime power in the port of Rotterdam—A feasibility study into the use of shore-side electricity for container ships moored at the Euromax terminal in Rotterdam," in *Port of Rotterdam Authority*, Rotterdam, The Netherlands: Havenbedrijf Rotterdam, Sep. 2006, p. 25. [Online]. Available: https://sustainableworldports.org/wp-content/uploads/Port-of-Rotterdam-Authority-Alternative-Maritime-Power-in-the-Port-of-Rotterdam.pdf

[9] A. Michail. (2020). *World Ports Initiatives on Climate Change Mitigation and Decarbonisation of Shipping*. [Online]. Available: https://unctad.org/system/files/non-official-document/cimem7_2020_P12_MICHAIL_en.pdf

[10] S. G. Jayasinghe, M. Al-Falahi, H. Enshaei, N. Fernando, and A. Tashakori, "Floating power platforms for mobile cold-ironing," in *Proc. IEEE 2nd Annu. Southern Power Electron. Conf. (SPEC)*, Dec. 2016, pp. 1–5, doi: 10.1109/SPEC.2016.7846221.

[11] C. Botana, "Best practices in the sustainable development of the ports—Port of Vigo: Green port," in *Proc. Atlantic Stakeholders Platform Conf.*, Porto, Portugal, Jan. 2015, pp. 1–14.

[12] A. Rolán, P. Manteca, R. Oktar, and P. Siano, "Integration of cold ironing and renewable sources in the Barcelona smart port," *IEEE Trans. Ind. Appl.*, vol. 55, no. 6, pp. 7198–7206, Nov. 2019, doi: 10.1109/TIA.2019.2910781.

[13] A. M. Kotrikla, T. Lilas, and N. Nikitakos, "Abatement of air pollution at an Aegean island port utilizing shoreside electricity and renewable energy," *Marine Policy*, vol. 75, pp. 238–248, 2017, doi: 10.1016/j.marpol.2016.01.026i.

[14] G. Caprara, V. Armas, D. de Mesquita Sousa, M. Kermani, and L. Martirano, "An energy storage system to support cruise ships cold ironing in the port of Civitavecchia," in *Proc. IEEE Int. Conf. Environ. Electr. Eng. IEEE Ind. Commercial Power Syst. Eur. (EEEIC/I&CPS Europe)*, Sep. 2021, pp. 1–5, doi: 10.1109/EEEIC/ICPSEurope51590.2021.9584733.

[15] P. Gemenetzis, E. Vranakis, K. Xydis, N. Sfakianos, S. Selas, and T. Sakaguchi, "Cold-ironing in anchorage area of Rotterdam port using renewable energy sources," in *Proc. SNAME Maritime Conv. 5th World Maritime Technol. Conf.*, 2015, doi: 10.5957/WMTC-2015-272.

[16] S. Wen, T. Zhao, Y. Tang, Y. Xu, M. Zhu, S. Fang, and Z. Ding, "Coordinated optimal energy management and voyage scheduling for all-electric ships based on predicted shore-side electricity price," *IEEE Trans. Ind. Appl.*, vol. 57, no. 1, pp. 139–148, Jan. 2021, doi: 10.1109/TIA.2020.3034290.

[17] Y. Tao, J. Qiu, S. Lai, X. Sun, and J. Zhao, "Flexible voyage scheduling and coordinated energy management strategy of all-electric ships and seaport microgrid," *IEEE Trans. Intell. Transp. Syst.*, vol. 24, no. 3, pp. 3211–3222, Mar. 2023, doi: 10.1109/TITS.2022.3226449.

[18] T. Zhao, J. Qiu, S. Wen, and M. Zhu, "Efficient onboard energy storage system sizing for all-electric ship microgrids via optimized navigation routing under onshore uncertainties," *IEEE Trans. Ind. Appl.*, vol. 58, no. 2, pp. 1664–1674, Mar. 2022, doi: 10.1109/TIA.2022.3145775.

[19] K. Hein, Y. Xu, G. Wilson, and A. K. Gupta, "Coordinated optimal voyage planning and energy management of all-electric ship with hybrid energy storage system," *IEEE Trans. Power Syst.*, vol. 36, no. 3, pp. 2355–2365, May 2021, doi: 10.1109/TPWRS.2020.3029331.

[20] R. Tang, X. Li, and J. Lai, "A novel optimal energy-management strategy for a maritime hybrid energy system based on large-scale global optimization," *Appl. Energy*, vol. 228, pp. 254–264, Oct. 2018, doi: 10.1016/j.apenergy.2018.06.092.

[21] Z. Li, Y. Xu, L. Wu, and X. Zheng, "A risk-averse adaptively stochastic optimization method for multi-energy ship operation under diverse uncertainties," *IEEE Trans. Power Syst.*, vol. 36, no. 3, pp. 2149–2161, May 2021, doi: 10.1109/TPWRS.2020.3039538.

[22] J. Wang, S. Chakraborty, V. Khatana, B. Lundstrom, G. Sarawat, and M. Salapaka, "Evaluation of optimal net load management in microgrids using hardware-in-the-loop simulation," in *Proc. IEEE Power Energy Soc. Innov. Smart Grid Technol. Conf. (ISGT)*, Apr. 2022, pp. 1–5.

[23] M. Kermani, E. Shirdare, G. Parise, M. Bongiorno, and L. Martirano, "A comprehensive technoeconomic solution for demand control in ports: Energy storage systems integration," *IEEE Trans. Ind. Appl.*, vol. 58, no. 2, pp. 1592–1601, Mar. 2022.

[24] H. Farzin, M. Fotuhi-Firuzabad, and M. Moeini-Aghtaie, "A stochastic multi-objective framework for optimal scheduling of energy storage systems in microgrids," *IEEE Trans. Smart Grid*, vol. 8, no. 1, pp. 117–127, Jan. 2017, doi: 10.1109/TSG.2016.2598678.

[25] J. E. Gutierrez-Romero, J. Esteve-Pérez, and B. Zamora, "Implementing onshore power supply from renewable energy sources for requirements of ships at berth," *Appl. Energy*, vol. 255, Dec. 2019, Art. no. 113883, doi: 10.1016/j.apenergy.2019.113883.

[26] N. N. A. Bakar, N. Bazmohammadi, Y. Yu, J. C. Vasquez, and J. M. Guerrero, "Environmental dispatch strategies for onshore power systems," in *Proc. IECON 48th Annu. Conf. IEEE Ind. Electron. Soc.*, Oct. 2022, pp. 1–4, doi: 10.1109/IECON49645.2022.9968795.

[27] B. O. Alawode, U. T. Salman, and M. Khalid, "A flexible operation and sizing of battery energy storage system based on butterfly optimization algorithm," *Electronics*, vol. 11, no. 1, p. 109, Dec. 2021, doi: 10.3390/electronics11010109.

[28] C. Li, F. de Bosio, F. Chen, S. K. Chaudhary, J. C. Vasquez, and J. M. Guerrero, "Economic dispatch for operating cost minimization under real-time pricing in droop-controlled DC microgrid," *IEEE J. Emerg. Sel. Topics Power Electron.*, vol. 5, no. 1, pp. 587–595, Mar. 2017, doi: 10.1109/JESTPE.2016.2634026.

[29] S. G. Gennitsaris and F. D. Kanellos, "Emission-aware and cost-effective distributed demand response system for extensively electrified large ports," *IEEE Trans. Power Syst.*, vol. 34, no. 6, pp. 4341–4351, Nov. 2019, doi: 10.1109/TPWRS.2019.2919949.

[30] F. D. Kanellos, E. M. Volanis, and N. D. Hatziargyriou, "Power management method for large ports with multi-agent systems," *IEEE Trans. Smart Grid*, vol. 10, no. 2, pp. 1259–1268, Mar. 2019, doi: 10.1109/TSG.2017.2762001.

[31] F. Conte, F. D'Agostino, D. Kaza, S. Massucco, G. Natrella, and F. Silvestro, "Optimal management of a smart port with shore-connection and hydrogen supplying by stochastic model predictive control," in *Proc. IEEE Power Energy Soc. Gen. Meeting (PESGM)*, Jul. 2022, pp. 1–5, doi: 10.1109/PESGM48719.2022.9916817.

[32] Q. Zhang, Q. Shan, and T. Li, "Large port energy management based on distributed optimization," in *Proc. 7th Int. Conf. Inf., Cybern., Comput. Social Syst. (ICCSS)*, Nov. 2020, pp. 108–113, doi: 10.1109/ICCSS52145.2020.9336919.

[33] *NSRDB: National Solar Radiation Database*, NREL, Golden, CO, USA. Accessed: Oct. 2022. [Online]. Available: https://nsrdb.nrel.gov/

[34] M. Sufyan, N. A. Rahim, C. Tan, M. A. Muhammad, and S. R. Sheikh Raihan, "Optimal sizing and energy scheduling of isolated microgrid considering the battery lifetime degradation," *PLoS ONE*, vol. 14, no. 2, Feb. 2019, Art. no. e0211642, doi: 10.1371/journal.pone.0211642.

[35] X. S. Yang, "Firefly algorithms for multimodal optimization," in *Stochastic Algorithms: Foundations and Applications*, vol. 5792. Berlin, Germany: Springer, 2009, doi: 10.1007/978-3-642-04944-6_14.

[36] *Electric Rates Table of KEPCO*. KEPCO, South Korea. Accessed: Jan. 2023. [Online]. Available: https://home.kepco.co.kr/kepco/EN/F/htmlView/ENFBHP00103.do?menuCd=EN060201

[37] P.-H. Tseng and N. Pilcher, "A study of the potential of shore power for the port of Kaohsiung, taiwan: To introduce or not to introduce?" *Res. Transp. Bus. Manage.*, vol. 17, pp. 83–91, Dec. 2015, doi: 10.1016/j.rtbm.2015.09.001.

[38] F. Adamo, G. Andria, G. Cavone, C. De Capua, A. M. L. Lanzolla, R. Morello, and M. Spadavecchia, "Estimation of ship emissions in the port of Taranto," *Measurement*, vol. 47, pp. 982–988, Jan. 2014, doi: 10.1016/j.measurement.2013.09.012.

[39] S. Fang, Y. Xu, Z. Li, T. Zhao, and H. Wang, "Two-step multi-objective management of hybrid energy storage system in all-electric ship microgrids," *IEEE Trans. Veh. Technol.*, vol. 68, no. 4, pp. 3361–3373, Apr. 2019.

[40] S. Fang, Y. Xu, Z. Li, Z. Ding, L. Liu, and H. Wang, "Optimal sizing of shipboard carbon capture system for maritime greenhouse emission control," *IEEE Trans. Ind. Appl.*, vol. 55, no. 6, pp. 5543–5553, Nov. 2019.

[41] Z. Li, Y. Xu, S. Fang, Y. Wang, and X. Zheng, "Multiobjective coordinated energy dispatch and voyage scheduling for a multienergy ship microgrid," *IEEE Trans. Ind. Appl.*, vol. 56, no. 2, pp. 989–999, Mar. 2020.

[42] M. D. A. Al-Falahi, K. S. Nimma, S. D. G. Jayasinghe, H. Enshaei, and J. M. Guerrero, "Power management optimization of hybrid power systems in electric ferries," *Energy Convers. Manage.*, vol. 172, pp. 50–66, Sep. 2018.

[43] A. A. Sheikh and D.-C. Lee, "Multi-stage multi-objective energy management system for seaport DC microgrids," in *Proc. 11th Int. Conf. Power Electron. ECCE Asia (ICPE-ECCE Asia)*, May 2023, pp. 335–340, doi: 10.23919/ICPE2023-ECCEAsia54778.2023.10213784.

[44] Y. Huang, H. Lan, Y.-Y. Hong, S. Wen, and S. Fang, "Joint voyage scheduling and economic dispatch for all-electric ships with virtual energy storage systems," *Energy*, vol. 190, Jan. 2020, Art. no. 116268.

[45] D. Gao, X. Wang, T. Wang, Y. Wang, and X. Xu, "An energy optimization strategy for hybrid power ships under load uncertainty based on load power prediction and improved NSGA-II algorithm," *Energies*, vol. 11, no. 7, p. 1699, Jul. 2018.

[46] A. De, S. K. Kumar, A. Gunasekaran, and M. K. Tiwari, "Sustainable maritime inventory routing problem with time window constraints," *Eng. Appl. Artif. Intell.*, vol. 61, pp. 77–95, May 2017.

[47] P. Xie, J. M. Guerrero, S. Tan, N. Bazmohammadi, J. C. Vasquez, M. Mehrzadi, and Y. Al-Turki, "Optimization-based power and energy management system in shipboard microgrid: A review," *IEEE Syst. J.*, vol. 16, no. 1, pp. 578–590, Mar. 2022, doi: 10.1109/JSYST.2020.3047673.

ADIL AYUB SHEIKH (Graduate Student Member, IEEE) received the B.E. degree in electrical engineering from the Anjuman College of Engineering and Technology, Nagpur, India, in 2016, and the M.Tech. degree in integrated power systems from the Visvesvaraya National Institute of Technology, Nagpur, in 2020. He is currently pursuing the Ph.D. degree with Yeungnam University, South Korea. His research interests include smart grids, microgrids, DC systems, renewable energy sources–control, protection, power quality, optimization, energy management, and grid-forming technology.

DONG-CHOON LEE (Senior Member, IEEE) received the B.S., M.S., and Ph.D. degrees in electrical engineering from Seoul National University, Seoul, South Korea, in 1985, 1987, and 1993, respectively.

He was a Research Engineer with Daewoo Heavy Industry, South Korea, from 1987 to 1988. He has been a Faculty Member with the Department of Electrical Engineering, Yeungnam University, Gyeongsan, South Korea, since 1994. He was a Visiting Scholar with the Power Quality Laboratory, Texas A&M University, College Station, TX, USA, in 1998; the Electrical Drive Center, University of Nottingham, Nottingham, England, U.K., in 2001; the Wisconsin Electric Machines and Power Electronics Consortium, University of Wisconsin, Madison, WI, USA, in 2004; and the FREEDM Systems Center, North Carolina State University, Raleigh, NC, USA, from September 2011 to August 2012. His current research interests include power converter design and control, renewable energy and its grid connection, AC machine drives, and DC power systems. He served as the General Chair for ICPE 2023-ECCE Asia held in Jeju, South Korea. He served as the Editor-in-Chief of *Journal of Power Electronics* of the Korean Institute of Power Electronics (KIPE) from January 2015 to December 2017. In 2019, he served as the President for KIPE. He is currently an Associate Editor of IEEE TRANSACTIONS ON POWER ELECTRONICS and an RDL of IEEE Power Electronics Society.